PM & FC

POWDER METALLURGY AND FUNCTIONAL COATINGS. 2023;17(3):55–66
Sergevnin V.S., Blinkov I.V., etc. Effect of HG40 and HS123 hard alloy tool substrates ...

Nanostructured Materials and Functional Coatings
Наноструктурированные материалы и функциональные покрытия

Effect of HG40 and HS123 hard alloy tool substrates on the properties of hardening coating

V. S. Sergevnin✉, I. V. Blinkov, D. S. Belov, A. P. Demirov, A. V. Chernogor, T. A. Lobova, A. I. Laptev

National University of Science and Technology "MISIS"
4 bld. 1 Leninskiy Prosp., Moscow 119049, Russia

✉ v.s.sergevnin@gmail.com

Abstract. This article examines the impact of surface and near-surface layer properties of a hard alloy on the physico-mechanical and tribological properties of Mo–Ti–Ni–Si–Al–N CAPVD-coatings deposited on HG40 and HS123 cutting tools. In both cases, the coatings had similar composition, multilayer architecture, and nanograin structure, with crystallite sizes ranging from 6 to 10 nm. However, there were significant differences in the hardness, elasticity modulus, and relative work of plastic deformation between the coatings. Specifically, on HG40 substrates, the hardness, elasticity modulus, and relative work of plastic deformation were equal to 27.6 GPa, 647 GPa and 38.2 %, respectively, while on HS123 substrates, they were 34.2 GPa, 481 GPa and 46.2 %, respectively. Furthermore, coatings formed on HS123 hard alloy demonstrated superior wear resistance and stronger adhesion. This can be attributed to the presence of higher compressive macrostresses within the coating. The maximum value of this property, approximately 5.2 GPa, was achieved when deposed to HS123 hard alloy, whereas the coating applied to HG40 reached a maximum value of approximately 3.2 GPa. Additionally, a more extensive diffusion zone between the substrate and coating components, along with associated structural phase heterogeneity, was observed at the coating-substrate interface when applied to HS123 substrate.

Keywords: coatings, arc-PVD, macrostresses, hardness, substrate–coating boundary

For citation: Sergevnin V.S., Blinkov I.V., Belov D.S., Demirov A.P., Chernogor A.V., Lobova T.A., Laptev A.I. Effect of HG40 and HS123 hard alloy tool substrates on the properties of hardening coating. *Powder Metallurgy and Functional Coatings*. 2023;17(3): 55–66. https://doi.org/10.17073/1997-308X-2023-3-55-66

Влияние твердосплавной инструментальной основы ВК10 и Т14К8 на свойства упрочняющего покрытия

В. С. Сергевнин✉, И. В. Блинков, Д. С. Белов, А. П. Демиров, А. В. Черногор, Т. А. Лобова, А. И. Лаптев

Национальный исследовательский технологический университет «МИСИС»
Россия, 119049, г. Москва, Ленинский пр-т, 4, стр. 1

✉ v.s.sergevnin@gmail.com

Аннотация. Исследовано влияние свойств поверхности и приповерхностного слоя твердого сплава на физико-механические и трибологические характеристики arc-PVD-покрытий Mo–Ti–Ni–Si–Al–N, нанесенных на твердосплавные пластины ВК10 и Т14К8. В обоих случаях покрытия характеризовались примерно одинаковым составом, многослойной архитектурой и нанозеренной структурой с размером кристаллитов 6–10 нм. При этом твердость, модуль упругости и относительная работа пластической деформации покрытий существенно отличались и составляли 27,6 ГПа, 647 ГПа, 38,2 % и 34,2 ГПа, 481 ГПа, 46,2 % соответственно на подложках ВК10 и Т14К8. Одновременно минимальный износ и повышенная

ПМ и ФП
ИЗВЕСТИЯ ВУЗОВ

ИЗВЕСТИЯ ВУЗОВ. ПОРОШКОВАЯ МЕТАЛЛУРГИЯ И ФУНКЦИОНАЛЬНЫЕ ПОКРЫТИЯ. 2023;17(3):55–66
Сергевнин В.С., Блинков И.В. и др. Влияние твердосплавной инструментальной основы ВК10 и Т14К8 ...

адгезионная прочность также были свойственны покрытиям, сформированным на твердом сплаве Т14К8. Обнаруженный эффект объясняется с позиции повышенных значений сжимающих макронапряжений, возникающих в покрытии. Значения данной характеристики для исследованного покрытия имели максимальное значение ~5,2 ГПа при нанесении на твердый сплав Т14К8 против ~3,2 ГПа для покрытия, нанесенного на ВК10. При этом наиболее протяженная диффузионная зона между компонентами подложки и покрытия и связанная с ней структурно-фазовая неоднородность формируются на границе покрытие–подложка при нанесении на подложку Т14К8.

Introduction

The studies conducted in the field of functional nanostructured surface coatings development have shown that multicomponent coating structures with different architectures based on nitrides exhibit superior operational performance compared to two and three component systems. These coatings possess enhanced elastic properties, resulting in greater resistance to plastic deformation. The inclusion of additional components in mononitride coatings leads to a reduction in average crystallite sizes and an increase in microdeformation, offering a potential approach to achieve coating materials that combine high hardness and resistance to destruction. Furthermore, these systems exhibit elevated heat resistance and thermal stability [1–5].

The fabrication process of Mo–Ti–Ni–Si–Al–N ion plasma arc vacuum coatings on heat resistant alloy substrates, as well as their properties, are discussed in reference [6]. The coating exhibits a multilayer structure consisting of nanograins with a crystallite size ranging from approximately 6 to 10 nm. The hardness of the coating is approximately 48 GPa, and it demonstrates high ratios of hardness to the Young modulus: $H/E = 0.12$ and $H^3/E^2 = 0.61$ GPa. These values indicate that the material has increased resistance to both elastic and plastic deformations [7; 8]. The coating shows a cohesive pattern of destruction when subjected to scribing, with partial substrate opening observed at an indenter load of approximately 70 N. Additionally, it is important to mention the tribological properties of the coating.

The combination of the aforementioned properties suggests that these coatings hold great potential for use as surface hardening for cutting tool [9–11]. However, the influence of the tool substrate's nature on the functional properties of these coatings remains unsolved. Several studies in this field have shown that the performance of substrate-coating composites is significantly affected by factors such as substrate composition, hardness, surface roughness, and the coefficients of thermal expansion of both the coating and the substrate.

This research aims to investigate the influence of two different types of hard alloys substrates on the properties of the hardening coating and the resulting substrate-coating composite. By examining the obtained results, we can determine the role of the substrate in shaping the functional properties of the coating and identify its most promising application.

Experimental

Coatings were applied to the surface of hard alloy substrates, specifically HG40 and HS123 hard alloy grades, which are commonly used for semifinal and rough milling [15; 16]. The coatings were fabricated using the arc-PVD method, which involves ion plasma vacuum arc spraying. The equipment used for this process included three evaporated cathodes (made of molybdenum, Al–Si alloy with 20 at. % and Ti–Ni alloy with 50 at. %). Toroidal electromagnetic separators were employed to prevent the deposition of sprayed material into the coating structure. To ensure uniform deposition, a kinematic rotating mechanism of the planetary type was used, rotating the substrates at a rate of 1 rpm with respect to the evaporated cathodes.

The coatings were deposited in a nitrogen atmosphere at $P_{N_2} \sim 3 \cdot 10^{-1}$ Pa. The electric arc current supplied to the evaporate cathodes was 120 A, while a negative bias voltage (U_c) –120 V was applied to the substrates. Prior to the coating deposition, the processed items' surfaces were subjected to preliminary gas abrasive processing using a mixture of air and corundum abrasive particles with a particle size distribution of 20–30 μm. This process resulted in a surface roughness of $R_a \sim 0.1$ μm. The thickness of the obtained coatings was 4 ± 0.1 μm.

The morphology of the coating was analyzed using JSM-7600F and JSM-6700F scanning electron microscopes (JEOL, Japan). The transversal cross-sec-

PM & FC

POWDER METALLURGY AND FUNCTIONAL COATINGS. 2023;17(3):55–66
Sergevnin V.S., Blinkov I.V., etc. Effect of HG40 and HS123 hard alloy tool substrates ...

tion structure of the Mo–Ti–Ni–Si–Al–N coatings was examined using a JEM-1400 transmission electron microscope, utilizing bright and dark field imaging, microdiffraction, and phase composition estimation.

X-ray photoelectron spectroscopy (XPS) was used to determine the bond energies of the elements present in the coating material, along with the simultaneous determination of their concentrations and the plotting of concentration profiles. This analysis was carried out using a Versa ProbeII device (ULVAC-PHI, Japan). Layer-by-layer analysis was conducted by spraying the coating surface with an argon ion beam with an energy of 2 keV and a 2×2 mm^2 grid, corresponding to an etching rate of 13 nm/min for SiO_2. The diameter of the analyzed region was 100 μm, and photoemission was excited using monochromatic AlK_α radiation with a power of 25 W. High-resolution photoelectron spectra were obtained with an analyzer transmission energy of 11.75 eV and a data acquisition density of 0.1 eV/step.

The diffusion zone at the interface between the coating and substrate was analyzed using electron Auger spectroscopy with a PHI-680 instrument (Physical Electronics, USA). Layer-by-layer ion etching of the material was performed using argon ions with energies of 1 and 2 keV at rates of approximately 5 and 20 nm/min, respectively, within a 1×1 mm grid and an incident angle of 60°.

The hardness (*H*) and elasticity modulus (*E*) of the Mo–Ti–Ni–Si–Al–N coatings applied to HG40 (WC–10Co) and HS123 (WC–14TiC–8Co) substrates were determined using continuous indentation in the load range of 5 to 100 mN, following the Oliver–Pharr method [17]. The relative work of plastic deformation was estimated based on the obtained loading-unloading curves, which was then used to estimate fracture toughness. The measurements were conducted with the indenter penetration depth not exceeding 10 % of the coating thickness to ensure that the material did not influence the determined parameters, in accordance with requirements of ISO/CD 14577.

The coefficient of friction and wear resistance parameters of the coatings were investigated using an automatic Tribometer friction machine (CSM Instruments, Switzerland). Tribological tests were conducted in a pin-on-disk configuration at ambient temperature in an air environment, using an Al_2O_3 counterbody. The normal contact load on the counterbody was 5 N, the friction velocity was set at approximately 10 cm/s, and the friction path length was 100 m. The wear intensity of the samples was determined through optical profilometry using a WYKO NT 1100 device («Veeco», USA).

The adhesion/cohesion strength in the coating–substrate system was estimated by performing scratching tests using a Revetest scratch tester (CSM Instruments, Switzerland). A series of scratches was applied to the coating surface using a diamond indenter with gradually increasing load up to 90 N. During this procedure, contact parameters such as acoustic emission (*AE*) from the contact area, force of friction between the indenter and sample surface (F_f) and the coefficient of friction (μ) were recorded. The critical loads, L_{c1} and L_{c3}, were determined, corresponding to the occurrence of the first scratch and the point at which the indenter made contact with the material, respectively. Additionally, the pattern of material destruction along the scratch was observed using optical microscopy.

The macrostresses in the coating, resulting from the difference in thermal expansion between the coating and substrate, as well as the different specific volume of phases, can be calculated using the Stoney equation. This equation is based on the curvature radius of the coating-substrate composite, which becomes curved due to these macrostresses. When the thickness of the coating is significantly smaller than the thickness of the substrate, the Stoney equation can be used to calculate the macrostresses caused by this difference in thermal expansion [18–21]:

$$\sigma = \frac{1}{6}\left(\frac{1}{R} - \frac{1}{R_0} \right)\frac{E_s t_s^2}{(1 - v_s) t_f}, \qquad (1)$$

where E_s represents the Young modulus of the substrate, GPa; v_s is the Poisson ratio of the substrate; R and R_0 are the curvature radii of the substrate before the application of the coating and after the deposition of the substrate-coating composite, respectively, m. The thicknesses of the substrate and coating are denoted by t_s and t_f, respectively, and they were determined by analyzing micro images of transversal fractures using a JSM-6700F scanning electron microscope.

To calculate the curvature radii of the blades before and after the deposition of the coating (R and R_0), profilograms of the sample surface were obtained using an optical profilometer. The following equation was used:

$$R = \frac{L^2}{8b}, \qquad (2)$$

where *L* represents the end-to-end length of the sample upon bending, m; *b* is the bending parameter.

Results and discussion

The surface morphology of the coatings obtained was characterized by a cellular structure, as depicted in

Figure 1. This structure was formed due to the replication of the relief of the substrate surface by the coating after undergoing preliminary gas abrasive treatment. The parameters of surface roughness (R_a) for all the coatings obtained were measured to be 0.10 ± 0.005 μm, indicating sufficiently uniform morphology.

The application of Arc-PVD Mo–Ti–Ni–Si–Al–N coatings on the utilized substrates resulted in coatings with a multilayer architecture, exhibiting a nanograin structure and crystallite sizes ranging from 6 to 10 nm (Figure 2).

The electron diffraction patterns of the coatings (Figure 3) reveal distinctive lines of electron diffraction. These lines can be attributed to both the TiN and Mo_2N phase due to the observed decrease in intraplane distances. This indicates the presence and consistent nature of the texture in the coatings formed on the two substrates, where the predominant crystallographic orientation of structural constituents aligns in the (100) direction, which corresponds to the direction of coating growth.

The elemental composition of the coatings was investigated using *X*-ray photoelectron spectroscopy (XPS), which provided data on the binding energy of the elements, enabling the determination of their phase composition. Table 1 presents the concentrations of elements in the coating at different depths after etching for 10 and 20 min. The experimental findings revealed the presence of regions within the coating structure enriched with various components. The periodical distribution of elements in the coatings was attributed to the rotation of substrates at a predetermined velocity relative to evaporated cathodes of specific composition. The laminar architecture of the coatings, as observed in Figure 2 using transmission electron spect-
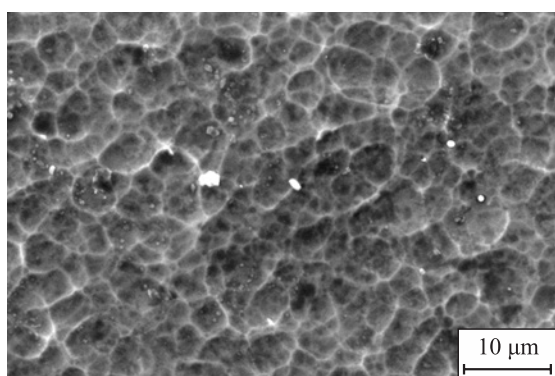
roscopy (TEM), was further confirmed by concentration profiles obtained during the layer-by-layer etching of the surface with argon ions (Figure 4).
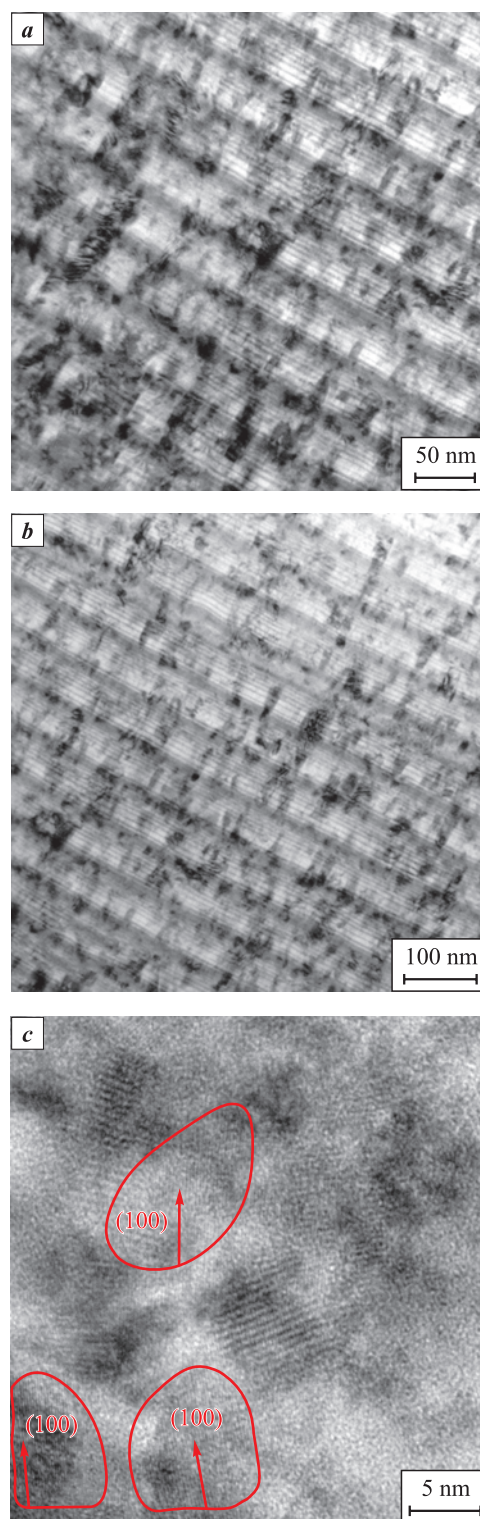

Fig. 1. SEM image of morphology
of Mo–Ti–Ni–Si–Al–N coating

Рис. 1. СЭМ-микрофотография морфологии
покрытия Mo–Ti–Ni–Si–Al–N

Fig. 2. TEM images of structure of Mo–Ti–Ni–Si–Al–N coatings
on carbide alloy substrates HG40 (*a*, *c*) and HS123 (*b*)

Рис. 2. ПЭМ-изображения структуры покрытий
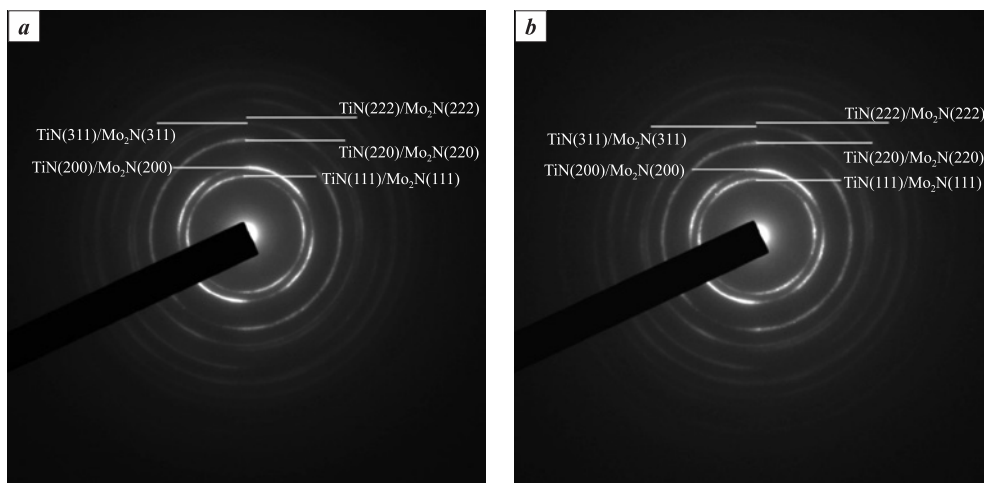Mo–Ti–Ni–Si–Al–N на твердосплавных основах
ВК10 (*a*, *c*) и Т14К8 (*b*)

Fig. 3. Electron diffraction patterns of Mo–Ti–Ni–Si–Al–N coating on HG40 (**a**) and HS123 (**b**)

Рис. 3. Электронограммы покрытия Mo–Ti–Ni–Si–Al–N на подложках ВК10 (**a**) и Т14К8 (**b**)

Table 1. **Composition of Mo–Ti–Ni–Si–Al–N coatings on carbide alloy substrates HG40 and HS123
after surface etching with argon ions during XPS (at the depth of ~130 and 260 nm)**

Таблица 1. **Состав покрытий Mo–Ti–Ni–Si–Al–N, сформированных на твердосплавных подложках
ВК10 и Т14К8 после травления поверхности ионами аргона в процессе РФЭС (на глубине ~130 и 260 нм)**

Etching duration, min	Concentration of elements, at. %						
	O	N	Ti	Mo	Ni	Al	Si
10	3.5 ± 0.1	45.0 ± 0.1	14.4 ± 0.1	30.0 ± 0.1	5.6 ± 0.1	1.5 ± 0.1	–
20	–	41.3 ± 0.1	8.3 ± 0.1	26.4 ± 0.1	4.7 ± 0.1	14.6 ± 0.1	4.7 ± 0.1

It is important to consider that XPS signal accumulation occurs from a region with a depth of several nanometers. As a result, the concentration profiles of coating elements obtained during the etching of the coating surface with argon ions may exhibit smoothed boundaries between individual layers [22]. This introduces some inconsistency in our understanding of the structure of the coatings, as observed through TEM data, which show well-defined layer boundaries, and XPS data, which exhibit smoothly varying concentration profiles of elements within the layers.

The coatings applied on two different substrates consisted of Mo_2N, AlN, Si_3N_4, TiN and Ni. This is supported by the analysis of energy spectra of photoelectrons from Mo 3d, Al 2p, Si 2p, Ti 2p and Ni 2p, which exhibit bond energies of 228.2 (3d5/2), 74.0, 102.2, 455.0 (Ti 2p3/2) and 853.1 (2p3/2) eV respectively [23–26].

Table 2 provides an overview of the hardness (H), elasticity modulus (E) and relative work of plastic deformation (W_p) for the coatings on different substrates.

The coatings that were obtained and had similar elemental and phase compositions when applied to different hard alloy substrates exhibited notable differences in terms of hardness. These differences were observed while adhering to the "ten percent" rule during hardness measurements [27]. However, despite the similar average coefficients of friction of approximately 0.6 observed during tribological tests (Figure 5), the wear of the coatings manifested in various manners.
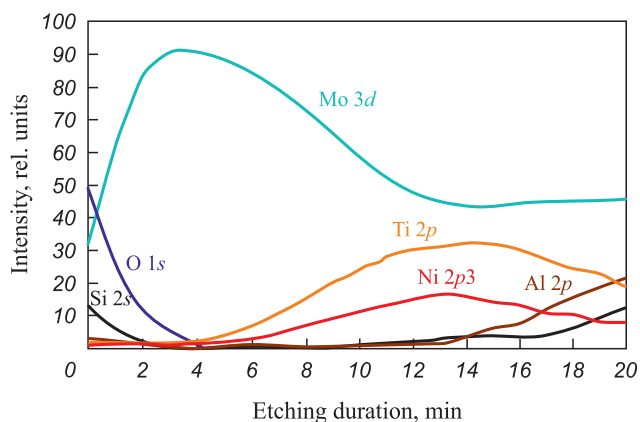

Fig. 4. Distribution of chemical elements in Mo–Ti–Ni–Si–Al–N coatings on carbide substrates during argon ion etching (nitrogen excluded)

Рис. 4. Распределение химических элементов в покрытии Mo–Ti–Ni–Si–Al–N на твердосплавных подложках в процессе травления ионами аргона (без учета азота)
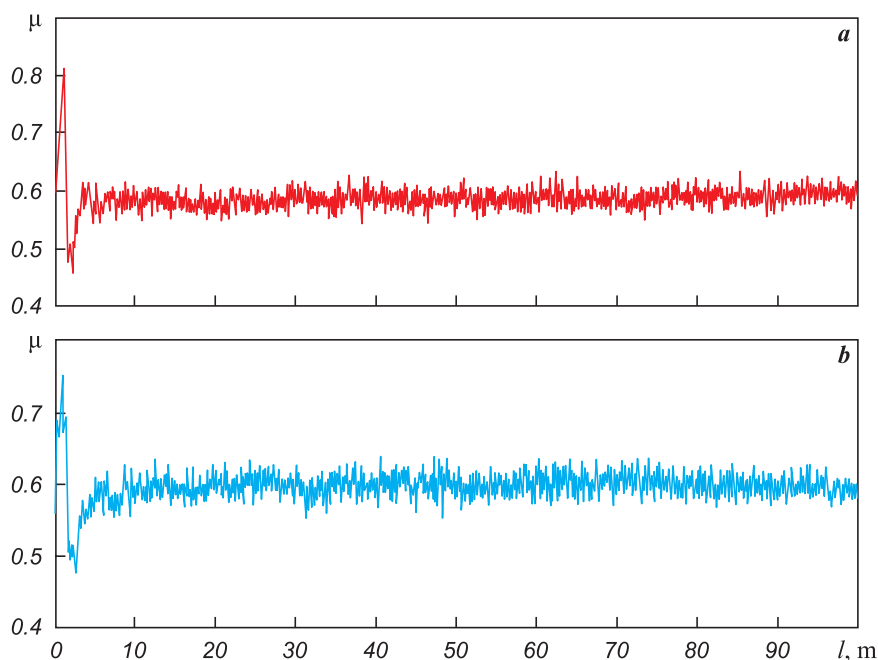
Fig. 5. Friction coefficient as a function of friction path for Mo–Ti–Ni–Si–Al–N coating
on HG40 (***a***) and HS123 (***b***) at a load of 5 N on Al_2O_3 counterbody

Рис. 5. Зависимость коэффициента трения от пути трения для покрытия Mo–Ti–Ni–Si–Al–N
на подложках ВК10 (***a***), Т14К8 (***b***) при нагрузке 5 Н на контртело из Al_2O_3

Based on the wear track profiles shown in Figure 6, it can be observed that the Mo–Ti–Ni–Si–Al–N coating on HS123 substrates experienced minimal wear, with the track depth comparable to the roughness of initial coating surface. On the other hand, the coatings on HG40 substrates exhibited wear of approximately $2.622 \cdot 10^{-5}$ mm^3/(N·m). These results can likely be attributed to the differing hardness of the Mo–Ti–Ni–Si–Al–N coating on the different substrates.

It is important to note that the nature of the substrate also plays a significant role in the adhesion between the coating and the substrate.

Table 2. **Physicomechanical properties of the considered samples of Mo–Ti–Ni–Si–Al–N coatings HG40 and HS123 substrates**

Таблица 2. **Физико-механические характеристики исследуемых образцов покрытий Mo–Ti–Ni–Si–Al–N и подложек ВК10 и Т14К8**

Substrate	E, GPa	H, GPa	W_p, %
Samples with coating			
HG40	647 ± 25	27.6 ± 1.1	38.2 ± 1.5
HS123	481 ± 19	34.2 ± 1.3	46.2 ± 1.8
Samples without coating			
HG40	574 ± 22	12.9 ± 0.5	–
HS123	520 ± 20	17.4 ± 0.7	–

Figure 7 depicts the variations in three recording parameters (AE, F_f and μ) in relation to the of scratch length and increasing load on the indenter during the measurement of the scratching process on the coatings applied to HG40 and HS123 substrates. The coatings in both series undergo destruction in multiple stages as a result of the diamond indenter. As the load
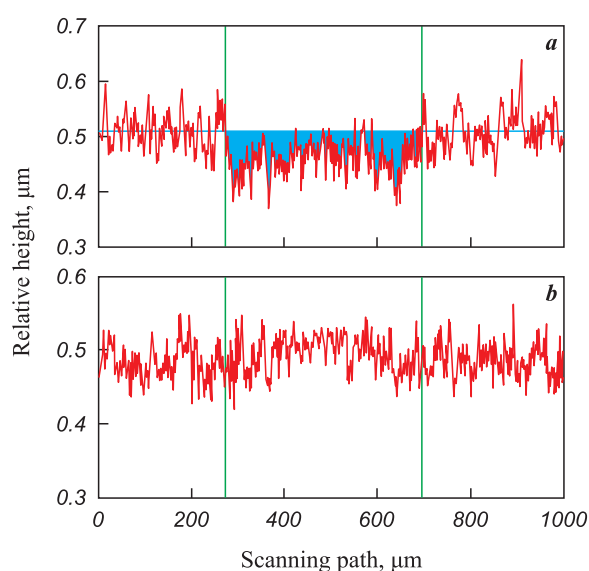

Fig. 6. Profilograms of wear tracks of Mo–Ti–Ni–Si–Al–N coating on HG40 (***a***) and HS123 (***b***) substrates

Рис. 6. Профилограммы дорожек износа покрытия Mo–Ti–Ni–Si–Al–N на подложках ВК10 (***a***) и Т14К8 (***b***)

PM & FC

POWER METALLURGY AND FUNCTIONAL COATINGS. 2023;17(3):55–66
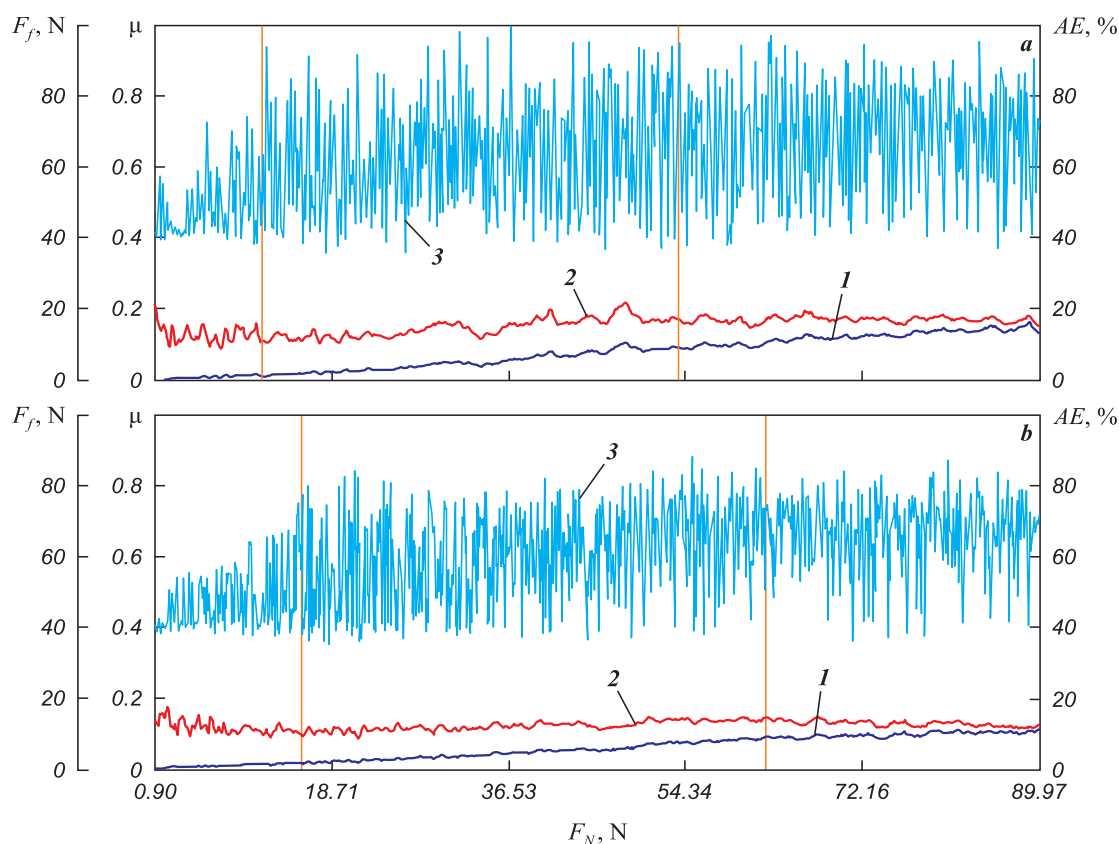*Sergevnin V.S., Blinkov I.V., etc.* Effect of HG40 and HS123 hard alloy tool substrates ...

Fig. 7. Friction force (F_f) (**1**), coefficient of friction (μ) (**2**), acoustic emission (*AE*) (**3**) during scratch test of Mo–Ti–Ni–Si–Al–N coatings on HG40 (**a**) and HS123 (**b**) substrates

Рис. 7. Зависимости силы трения (F_f) (**1**), коэффициента трения (μ) (**2**), акустической эмиссии (*AE*) (**3**) при скретч-тесте покрытий Mo–Ti–Ni–Si–Al–N на подложках ВК10 (**a**) и Т14К8 (**b**)

increases, the indenter progressively penetrates into the coating, eliminating surface irregularities and intermittently contacting the surface. During this stage, the signal amplitude of acoustic emission exhibits an increase, while the intensity remains relatively constant, albeit at a negligible level.

A significant drop in amplitude (*AE*) occurs at loads of approximately 11.7 and 15.6 N (L_{c1}) on the indenter for both HG40 and HS123 coatings, as shown in Figure 7. This drop indicates the initiation of the first cracks in the coating. Visual examination of the scratch bottom (Figure 8) confirms the presence of cracks and detachment of coating fragments. Partial wear of the coatings on HG40 and HS123 substrates occurs at loads (L_{c3}) on the indenter of approximately 53.7 and 62.5 N, respectively. Simultaneously, the slope angle of the force F_f curve (*1*) and the coefficient of friction μ (*2*) change as a function of the applied load (refer to Fig. 7). These changes are attributed to the penetration of the indenter into the substrate, which has a lower hardness compared to the coating material.

The hardness, wear, and adhesion of coatings with the same composition, thickness, and structural proper-ties were found to be influenced by the nature of the substrate onto which they were deposited. To investigate this phenomenon, macrostressed states in the formed coating-substrate composites were analyzed.

In this analysis, sufficiently thin substrates were fabricated from the considered hard alloys, with average thicknesses of approximately 425.12 μm and 449.67 μm, respectively. Mo–Ti–Ni–Si–Al–N coatings of the aforementioned compositions, with thicknesses ranging from 4.11 to 4.21 μm, were then applied onto these substrates. The curvature radii were measured before and after the deposition of the coatings. By employing Equation (1) and utilizing published data on the Poisson ratios of the hard alloy substrates, as well as experimentally obtained elasticity moduli of the substrates (as shown in Table 3), the macrostresses (σ) in the coatings were calculated. The results of these calculations are summarized in Table 3. As evident from the presented results, the coatings formed on HS123 substrates exhibited the highest values of σ, indicating the presence of high levels of compressive macrostresses. These compressive macrostresses can account for the elevated hardness of the coatings on these substrates, which, in turn, influ-
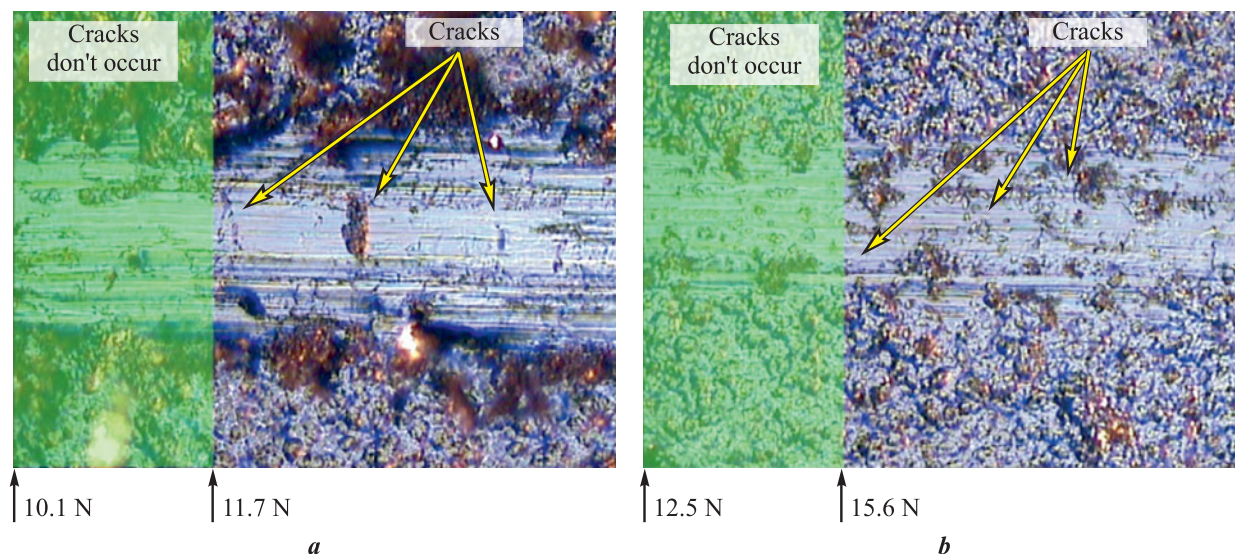
ПМ и ФП
ИЗВЕСТИЯ ВУЗОВ

ИЗВЕСТИЯ ВУЗОВ. ПОРОШКОВАЯ МЕТАЛЛУРГИЯ И ФУНКЦИОНАЛЬНЫЕ ПОКРЫТИЯ. 2023;17(3):55–66
Сергевнин В.С., Блинков И.В. и др. Влияние твердосплавной инструментальной основы ВК10 и Т14К8 ...

Fig. 8. Images of a scratch fragment formed during the scratch test of Mo–Ti–Ni–Si–Al–N nanostructured coatings on HG40 (***a***) and HS123 (***b***) substrates upon increasing load on indenter

Рис. 8. Изображения участка царапины, формирующейся в процессе скретч-теста наноструктурных покрытий Mo–Ti–Ni–Si–Al–N на подложках ВК10 (***a***) и Т14К8 (***b***) при увеличивающейся нагрузке на индентор

ences their wear resistance [28; 29]. The significant role of compressive macrostresses in relation to coating hardness is further supported by the experimental findings of other researchers [30–35].

The higher adhesion strength observed for Mo–Ti–Ni–Si–Al–N coatings on HS123 substrates, compared to HG40 substrates, can be attributed to the relatively higher macrostresses achieved in the former case. These macrostresses can have a significant impact on the nucleation and propagation of cracks during scribing in the relatively brittle coating material (L_{c1}) as well as on the subsequent fragmentation of its continuous layer and the opening of the substrate (L_{c2}) [36; 37].

The observed differences in macrostresses between the considered coatings on HG40 and HS123 hard alloy substrates, despite their relatively equal coefficients of linear thermal expansion ($5.8 \cdot 10^{-6}$ and $6.0 \cdot 10^{-6}$ K^{-1} respectively), owhich determine the thermal component of macrostresses, may be associated with the structural phase (concentration) heterogeneity of the coating material, including the transitional zone between the coating and substrate. Auger spectrometry was employed to analyze the regions adjacent to the coating-substrate interface for the two substrates.

Figure 9 illustrates the concertation profiles of the distribution of elements, which are components of both the substrate and the coating, in boundary regions. From the presented results, it can be inferred that the size of the diffusion region is maximized at the Mo–Ti–Ni–Si–Al–N coating–HS123 alloy composite, with a size of approximately 1.55 μm, compared to its size of approximately 0.82 μm for the HG40 substrate.

The larger size of the diffusion zone in the Mo–Ti–Ni–Si–Al–N coating on HS123 substrate is the reason behind the higher macrostresses detected, primarily due to its concentration constituents. This is further supported by the longer length of the transient zone at the interface between the growing coat-

Table 3. Macrostresses calculated by the Stoney method achieved in Mo–Ti–Ni–Si–Al–N-coating–substrate composite

Таблица 3. Результаты расчета методом Стони макронапряжений, реализующихся в композите «Mo–Ti–Ni–Si–Al–N-покрытие–подложка»

| Substrate	σ_{calc}, GPa	R, m	R_0, m	t_s, 10^{-6} m	t_f, 10^{-6} m	ν_s	E_s, GPa
HG40	–2.9	3.55	1.69	449.67	4.21	0.22	574
HS123	–5.2	4.75	1.08	420.52	4.15	0.21	520
Notations: σ_{calc} – calculated macrostresses; R – substrate curvature radius before application of coating; R_0 – curvature radius of coating–substrate composite; t_s – substrate thickness; t_f – coating thickness; ν_s – Poisson ratio of substrate; E_s – substrate elasticity modulus.							
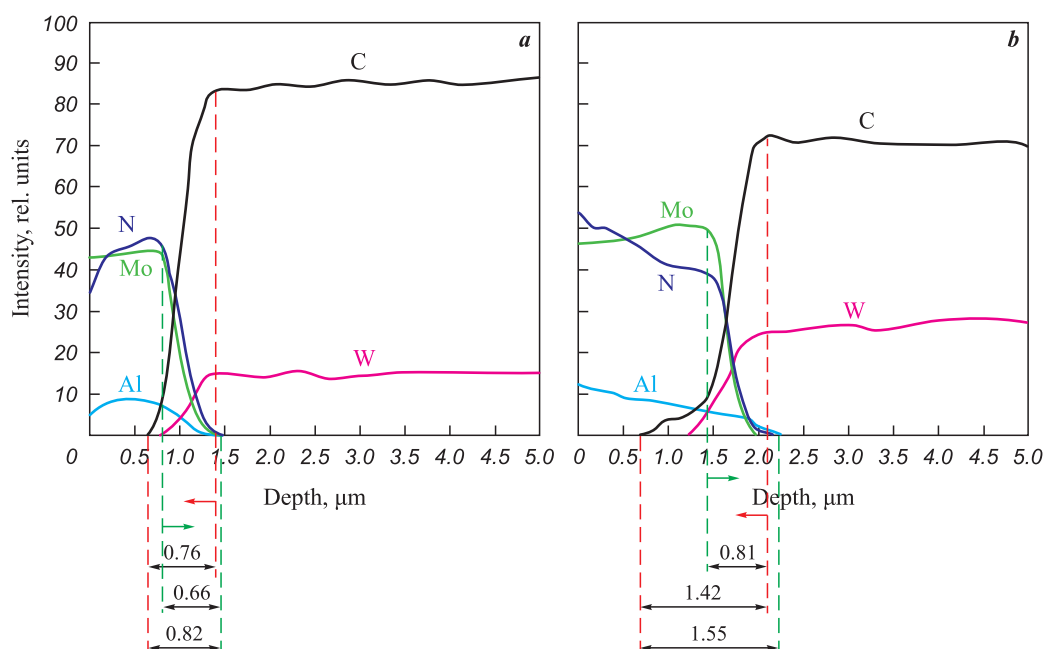
Fig. 9. Distribution of elements in Mo–Ti–Ni–Si–Al–N coating and HG40 (*a*) and HS123 (*b*) substrates
at the coating–substrate interfaces

Рис. 9. Распределение элементов покрытия Mo–Ti–Ni–Si–Al–N и подложек ВК10 (*a*) и Т14К8 (*b*)
на границах раздела покрытие–подложка

ing and the HS123 substrate. This longer length can be attributed to a local increase in the temperature of this region during the formation of the coating, which is caused by the lower heat conductivity of the HS123 substrate compared to the HG40 substrate [38; 39]. The lower heat conductivity of the HS123 substrate, in comparison that of the HG40 material, approximately 67 W/(m·K), results in insufficient heat removal from the zone of heat release during coating formation. This heat release is caused by the absorption of latent heat released during ion braking, condensation of vapor atoms, and heat transfer by radiation from the vaporizer. As a result, the heat is not effectively dissipated, leading to a localized increase in temperature in the transient zone.

Conclusions

The Mo–Ti–Ni–Si–Al–N hardening coating, characterized by a multilayer architecture with a nanograin structure and crystallite sizes of 6–10 nm, was deposited onto HG40 and HS123 hard alloy substrates using ion plasma vacuum arc deposition. The resulting nano-indentation measurements indicated a hardness of 27.6 GPa and an elasticity modulus of 647 GPa for HG40, accompanied by a relative work of plastic deformation of 38.2 %. Likewise, for HS123, the coating demonstrated a hardness of 34.2 GPa, an elasticity modulus of 481 GPa, and a relative work of plastic deformation of 46.2 %.

The coatings obtained, with roughly equivalent elemental and phase compositions, when applied to diverse hard alloy substrates and meeting the "ten percent" rule in nano-indentation, exhibited distinct physicochemical properties. Specifically, the Mo–Ti–Ni–Si–Al–N coating on the HS123 hard alloy substrate displayed the highest hardness and the lowest wear, along with superior adhesion strength. This phenomenon can be attributed to the achievement of maximum compressive macrostresses within the coating (approximately 5.2 GPa) in this particular case, surpassing the coatings with similar compositions on HG40 substrates (approximately 2.9 GPa). The observed variation in physicochemical properties, despite the relatively small difference in coefficients of linear thermal expansion between the hard alloy substrates, can be attributed to the presence of a diffusion zone of greater length at the interface between the substrate and coating. This diffusion zone, along with accompanying structural phase heterogeneities, influences the magnitude of concentration macrostresses that contribute to the hardening of the coating.

References / Список литературы

1. Pogrebnjak A.D., Eyidi D., Abadias G., Bondar O.V., Beresnev V.M., Sobol O.V. Structure and properties of arc evaporated nanoscale TiN/Mon multilayered systems. *International Journal of Refractory Metals and Hard Materials*. 2015;48:222–228.
https://doi.org/10.1016/j.ijrmhm.2014.07.043

2. Chang H.-W., Huang P.-K., Yeh J.-W., Davison A., Tsau C.-H., Yang C.-C. Influence of substrate bias, deposition temperature and post-deposition annealing on the structure and properties of multi-principal-component (AlCrMoSiTi)N coatings. *Surface and Coatings Technology*. 2008;202(14): 3360–3366. https://doi.org/10.1016/j.surfcoat.2007.12.014

3. Lai C.-H., Cheng K.-H., Li S.-J., Yeh J.-W. Mechanical and tribological properties of multi-element (AlCrTaTiZr)N coatings. *Surface and Coatings Technology*. 2008;202(15): 3732–3738. https://doi.org/10.1016/j.surfcoat.2008.01.014

4. Sergevnin V.S., Blinkov I.V., Volkhonskii A.O., Belov D.S., Kuznetsov D.V., Gorshenkov M.V., Skryleva E.A. Wear behaviour of wear-resistant adaptive nano-multilayered Ti–Al–Mo–N coatings. *Applied Surface Science*. 2016;388;Part A:13–23. https://doi.org/10.1016/j.apsusc.2016.06.102

5. Vereschaka A., Grigoriev S., Sitnikov N., Batako A. Delamination and longitudinal cracking in multi-layered composite nanostructured coatings and their influence on cutting tool life. *Wear*. 2017;390–391:209–219. https://doi.org/10.1016/j.wear.2017.07.021

6. Blinkov I.V., Volkhonskii A.O., Chernogor A.V., Sergevnin V.S., Belov D.S., Polyanskii A.M. Structure, composition, and properties of Arc PVD Mo–Si–Al–Ti–Ni–N coatings. *Inorganic Materials*. 2018;54(5):437–445. https://doi.org/10.1134/S0020168518050023

   Блинков И.В., Волхонский А.О., Черногор А.В., Сергевнин В.С., Белов Д.С., Полянский А.М. Структура, состав и свойства ионно-плазменных вакуумно-дуговых покрытий Mo–Si–Al–Ti–Ni–N. *Неорганические материалы*. 2018;54(5):458–466. https://doi.org/10.7868/S0002337X18050056

7. Leyland A., Matthews A. On the significance of the *H/E* ratio in wear control: A nanocomposite coating approach to optimized tribological behavior. *Wear*. 2000;246(1-2): 1–11. https://doi.org/10.1016/S0043-1648(00)00488-9

8. Tsui T.Y., Pharr G.H., Oliver W.C., White W.C. Nanoindentation and nanoscratching of hard carbon coatings for magnetic disks. *MRS Online Proceedings Library*. 1995;383(1):447–452. https://doi.org/10.1557/PROC-383-447

9. Veprek S., Holubar P., Veprek-Heijman M. Industrial applications of hard and superhard nanocomposite coatings on tools for machining, forming, stamping and injection molding. *Advanced Materials Research*. 2016;1135:218–233. https://doi.org/10.4028/www.scientific.net/AMR.1135.218

10. Fox-Rabinovich G., Yamamoto K., Beake B., Gershman I., Kovalev A., Veldhuis S., Aguirre M., Dosbaeva G., Endrino J. Hierarchical adaptive nanostructured PVD coatings for extreme tribological applications: the quest for nonequilibrium states and emergent behavior. *Science and Technology of Advanced Materials*. 2012;13(4):043001. https://doi.org/10.1088/1468-6996/13/4/043001

11. Sergevnin V.S., Blinkov I.V., Belov D.S., Smirnov N.I., Volkhonskii A.O., Kuptsov K.A. Wear and erosion of arc-PVD multilayer Ti–Al–Mo–N coatings under various conditions of friction and loading. *The International Journal of Advanced Manufacturing Technology*. 2018;98(1): 593–601. https://doi.org/10.1007/s00170-018-2235-z

12. Shima M., Okado J., McColl I.R., Waterhouse R.B., Hasegawa T., Kasaya M. The influence of substrate material and hardness on the fretting behaviour of TiN. *Wear*. 1999;225-229:38–45. https://doi.org/10.1016/S0043-1648(99)00062-9

13. Drábik M., Truchlý M., Ballo V., Roch T., Kvetková L., Kúš P., Influence of substrate material and its plasma pretreatment on adhesion and properties of WC/a-C:H nanocomposite coatings deposited at low temperature. *Surface and Coatings Technology*. 2018;333:138–147. https://doi.org/10.1016/j.surfcoat.2017.10.081

14. Seidl W.M., Bartosik M., Kolozsvári S., Bolvardi H., Mayrhofer P. H. Influence of coating thickness and substrate on stresses and mechanical properties of (Ti,Al,Ta)N/(Al,Cr)N multilayers. *Surface and Coatings Technology*. 2018;347:92–98. https://doi.org/10.1016/j.surfcoat.2018.04.060

15. Kagnaya T., Boher C., Lambert L., Lazard M., Cutard T. Wear mechanisms of WC–Co cutting tools from high-speed tribological tests. *Wear*. 2009;267(5-8):890–897. https://doi.org/10.1016/j.wear.2008.12.035

16. Weidow J., Zackrisson J., Jansson B., Andréna H.-O. Characterisation of WC–Co with cubic carbide additions. *International Journal of Refractory Metals and Hard Materials*. 2009;27(2):244–248. https://doi.org/10.1016/j.ijrmhm.2008.11.007

17. Oliver W.C., Pharr G.M., An improved technique for determining hardness and elastic modulus. *Journal of Materials Research*. 1992;7(6):1564–1583. https://doi.org/10.1557/JMR.1992.1564

18. Stoney G.G. The tension of metallic films deposited by electrolysis. *Proceedings of the Royal Society A*. 1909;82(553):172–175. https://doi.org/10.1098/rspa.1909.0021

19. Pureza J.M., Lacerda M.M., De Oliveira A.L., Fragalli J.F., Zanon R.A.S. Enhancing accuracy to Stoney equation. *Applied Surface Science*. 2009;255(12):6426–6428. https://doi.org/10.1016/j.apsusc.2009.01.097

20. Blinkov I.V., Volkhonskii A.O., Belov D.S., Sergevnin V.S., Chernogor A.V., Kiseleva T.V., Bondarev A.V. Superhard nanostructured ceramic–metal coatings with a low macrostress level. *Technical Physics Letters*. 2018;44(2): 167–169. https://doi.org/10.1134/S1063785018020165

   Блинков И.В., Волхонский А.О., Белов Д.С., Сергевнин В.С., Черногор А.В., Киселева Т.В., Бондарев А.В. Высокотвердые наноструктурные керамико-металлические покрытия с низким уровнем макронапряжений. *Письма в журнал технической физики*. 2018;(4):80–86. http://dx.doi.org/10.21883/PJTF.2018.04.45642.17083

21. Shiri S., Ashtijoo P., Odeshi A., Yang Q. Evaluation of Stoney equation for determining the internal stress of DLC thin films using an optical profiler. *Surface and Coatings Technology*. 2016;308:98–100. http://dx.doi.org/10.1016/j.surfcoat.2016.07.098

22. Chernogor A.V., Blinkov I.V., Belov D.S., Sergevnin V.S., Volkhonskii A.O. Analysis of the structure of multilayer nanocrystalline coatings based on plasma mass transfer parameters calculated by the monte carlo

method. *Technical Physics Letters*. 2019;45(2):75–81. https://doi.org/10.1134/S1063785019020056

Черногор А.В., Блинков И.В., Белов Д.С., Сергевнин В.С., Волхонский А.О. Анализ структуры многослойных нанокристаллических покрытий на основе параметров массопереноса плазмы, вычисленных методом Монте-Карло. *Письма в журнал технической физики*. 2019;(3):16–20. http://dx.doi.org/10.21883/PJTF.2019.03.47265.17575

23. Bertóti I. Characterization of nitride coatings by XPS. *Surface and Coatings Technology*. 2002;151-152:194–203. https://doi.org/10.1016/S0257-8972(01)01619-X

24. Crist B.V. Handbook of the elements and native oxides. California: LLC XPS International, 1999. 560 p.

25. Sanjines R., Wiemer C., Almeida J., Levy F. Valence band photoemission study of the Ti–Mo–N system. *Thin Solid Films*. 1996;290-291:334–338. https://doi.org/10.1016/S0040-6090(96)09082-7

26. Wang T., Zhang G., Ren S., Jiang B. Effect of nitrogen flow rate on structure and properties of MoN_x coatings deposited by facing target sputtering, *Journal of Alloys and Compounds*. 2017;701:1–8. http://dx.doi.org/10.1016/j.jallcom.2017.01.077

27. Pharr G.M., Oliver W.C. Measurement of thin-film mechanical properties using nanoindentation. *MRS Bulletin*. 1992;17(7):28–33. https://doi.org/10.1557/S0883769400041634

28. Mayrhofer P.H., Mitterer C., Hultman L., Clemens H. Microstructural design of hard coatings. *Progress in Materials Science*. 2006;51(8):1032–1114. https://doi.org/10.1016/j.pmatsci.2006.02.002

29. Veprek S., Veprek-Heijman M.G.J., Karvankova P., Prochazka J. Different approaches to superhard coatings and nanocomposites. *Thin Solid Films*. 2009;476(1):1–29. https://doi.org/10.1016/j.tsf.2004.10.053

30. Kulikovsky V., Bohac P., Franc F., Deineka A., Vorlicek V., Jastrabik L. Hardness, intrinsic stress, and structure of the a-C and a-C:H films prepared by magnetron sputtering. *Diamond and Related Materials*. 2001;10(3-7):1076–1081. https://doi.org/10.1016/S0925-9635(00)00525-2

31. Mayrhofer P.H., Tischler G., Mitterer C. Microstructure and mechanical/thermal properties of Cr–N coatings by reactive unbalanced magnetron sputtering. *Surface and Coatings Technology*. 2001;142–144:78–84. https://doi.org/10.1016/S0257-8972(01)01090-8

32. Mayrhofer P.H., Kunc F., Musil J., Mitterer C. A comparative study on reactive and nonreactive unbalanced magnetron sputter deposition of TiN coatings. *Thin Solid Films*. 2001;415(1–2):151–159. https://doi.org/10.1016/S0040-6090(02)00511-4

33. Rickerby D.S. Internal stress and adherence of titanium nitride coatings. *Journal of Vacuum Science & Technology A*. 1986;4(6):2809–2814. https://doi.org/10.1116/1.573683

34. Window B., Harding G.L., Horrigan C., Bell T. Stress and microhardness in sputter deposited molybdenum and chromium films. *Journal of Vacuum Science & Technology A*. 1992;10(5):3278–3282. https://doi.org/10.1116/1.577855

35. Jaroš M., Musil J., Haviar S. Interrelationships among macrostress, microstructure and mechanical behavior of sputtered hard Ti(Al,V)N films. *Materials Letters*. 2019;235:92–96. https://doi.org/10.1016/j.matlet.2018.09.173

36. Wang Q., Zhou F., Zhou Z., Li L. K.-Y., Yan J. An investigation on the crack resistance of CrN, CrBN and CrTiBN coatings via nanoindentation. *Vacuum*. 2017;145:186–193. https://doi.org/10.1016/j.vacuum.2017.08.041

37. Vereschaka A.A., Grigoriev S.N. Study of cracking mechanisms in multi-layered composite nano-structured coatings. *Wear*. 2017;378-379:43–57. http://dx.doi.org/10.1016/j.wear.2017.01.101

38. Davis J.R. Tool materials: ASM Specialty Handbook. ASM International, 1995. 501 p.

39. Schultrich B., Poeßnecker W., Thermal conductivity of cemented carbides. *Journal of Thermal Analysis and Calorimetry*. 1998;33(1):305–310. https://doi.org/10.1007/BF01914616

Information about the Authors

Viktor S. Sergevnin – Cand. Sci. (Eng.), Master of Teaching, Department of Functional Nanosystems and High-Temperature Materials, National University of Science and Technology "MISIS" (NUST MISIS).
ORCID: 0000-0002-4007-435X
E-mail: v.s.sergevnin@gmail.com

Igor V. Blinkov – Dr. Sci. (Eng.), Professor, Department of Functional Nanosystems and High-Temperature Materials, NUST MISIS.
ORCID: 0000-0001-8619-6259
E-mail: biv@misis.ru

Dmitry S. Belov – Cand. Sci. (Eng.), Master of Teaching, Department of Functional Nanosystems and High-Temperature Materials, NUST MISIS.
ORCID: 0000-0002-7053-5540
E-mail: dm.blv@yandex.ru

Сведения об авторах

Виктор Сергеевич Сергевнин – к.т.н., учебный мастер кафедры функциональных наносистем и высокотемпературных материалов, Национальный исследовательский технологический университет «МИСИС» (НИТУ МИСИС).
ORCID: 0000-0002-4007-435X
E-mail: v.s.sergevnin@gmail.com

Игорь Викторович Блинков – д.т.н., профессор кафедры функциональных наносистем и высокотемпературных материалов, НИТУ МИСИС.
ORCID: 0000-0001-8619-6259
E-mail: biv@misis.ru

Дмитрий Сергеевич Белов – к.т.н., учебный мастер кафедры функциональных наносистем и высокотемпературных материалов, НИТУ МИСИС.
ORCID: 0000-0002-7053-5540
E-mail: dm.blv@yandex.ru

![ПМ и ФП ИЗВЕСТИЯ ВУЗОВ]

ИЗВЕСТИЯ ВУЗОВ. ПОРОШКОВАЯ МЕТАЛЛУРГИЯ И ФУНКЦИОНАЛЬНЫЕ ПОКРЫТИЯ. 2023;17(3):55–66
Сергевнин В.С., Блинков И.В. и др. Влияние твердосплавной инструментальной основы ВК10 и Т14К8 ...

Alexander P. Demirov – Laboratory Assistant-Researcher, Department of Functional Nanosystems and High-Temperature Materials, NUST MISIS.
ⓘ *ORCID*: 0000-0002-5014-2993
✉ *E-mail:* apdemirov@gmail.com

Aleksey V. Chernogor – Master of Teaching, Department Functional Nanosystems and High-Temperature Materials, NUST MISIS.
ⓘ *ORCID*: 0000-0001-5385-5369
✉ *E-mail:* avchernogor@gmail.com

Tamara A. Lobova – Dr. Sci. (Eng.), Professor, Export Control Specialist, NUST MISIS.
✉ *E-mail:* smazka39@mail.ru

Alexander I. Laptev – Dr. Sci. (Eng.), Chief Researcher, Research Laboratory of Superhard Materials, NUST MISIS.
✉ *E-mail:* laptev@misis.ru

Александр Павлович Демиров – лаборант-исследователь кафедры функциональных наносистем и высокотемпературных материалов, НИТУ МИСИС.
ⓘ *ORCID*: 0000-0002-5014-2993
✉ *E-mail:* apdemirov@gmail.com

Алексей Витальевич Черногор – учебный мастер кафедры функциональных наносистем и высокотемпературных материалов, НИТУ МИСИС.
ⓘ *ORCID*: 0000-0001-5385-5369
✉ *E-mail:* avchernogor@gmail.com

Тамара Александровна Лобова – д.т.н., профессор, специалист по экспортному контролю, НИТУ МИСИС.
✉ *E-mail:* smazka39@mail.ru

Александр Иванович Лаптев – д.т.н., гл. науч. сотрудник научно-исследовательской лаборатории сверхтвердых материалов, НИТУ МИСИС.
✉ *E-mail:* laptev@misis.ru

Contribution of the Authors / Вклад авторов

V. S. Sergevnin – formulated a the basic concept, formulated the purpose and objectives of the study, prepared the manuscript, formulated conclusions, studied the structure and composition of coatings and macrostressed state of samples with coatings.
I. V. Blinkov – scientific advising, edited the manuscript and conclusions.
D. S. Belov – analyzed the research results, prepared the illustrative material, conducted experiments on the physicomechanical properties of coatings.
A. P. Demirov – conducted research on the structure and composition of coatings, provided resources.
A. V. Chernogor – conducted experiments on deposition of coatings.

T. A. Lobova – conducted tribological studies of samples with coatings.
A. I. Laptev – studied the adhesive strength of coatings with carbide substrate.

В. С. Сергевнин – формирование основной концепции, постановка цели и задачи исследования, подготовка текста, формулирование выводов, проведение исследований макронапряженного состояния образцов с покрытиями.
И. В. Блинков – научное руководство, редактирование текста и выводов.
Д. С. Белов – анализ результатов исследований, подготовка иллюстративного материала, проведение экспериментов по изучению физико-механических свойств покрытий.
А. П. Демиров – проведение исследований структуры и состава покрытий, обеспечение ресурсами.
А. В. Черногор – проведение экспериментов по осаждению покрытий.
Т. А. Лобова – проведение трибологических исследований образцов с покрытиями.
А. И. Лаптев – исследования адгезионной прочности покрытий с твердосплавной подложкой.